1 # Detection of microplastics in ambient particulate matter using Raman Spectral
2 # Imaging and chemometric analysis

3 Joseph M. Levermore[1*], Thomas E L Smith[2,3], Frank J. Kelly[1] and Stephanie L. Wright[1]

4 [1]MRC Centre for Environment and Health, Department of Analytical, Environmental and Forensic
5 Sciences, King's College London, London SE1 9NH, United Kingdom.

6 [2]Department of Geography, King's College London, Strand, London, WC2R 2LS, United Kingdom.

7 [3]Department of Geography and Environment, London School of Economics and Political Science,
8 Houghton Street, London WC2A 2AE, United Kingdom.

9 ## **Abstract**

10 Microplastics have been observed in indoor and outdoor air. This raises concern for human exposure,
11 especially should they occur in small enough sizes, which if inhaled, reach the central airway and distal
12 lung. As yet, methods for their detection have not spectroscopically verified the chemical composition
13 of microplastics in this size-range. One proposed method is an automated spectroscopic technique,
14 Raman spectral imaging; however, this generates large and complex data sets. This study aims to
15 optimize Raman spectral imaging for the identification of microplastics (≥2 μm) in ambient particulate
16 matter, using different chemometric techniques. We show that Raman spectral images analyzed using
17 chemometric statistical approaches are appropriate for the identification of both virgin and
18 environmental microplastics ≥2 μm in size. On the basis of the sensitivity, we recommend using the
19 developed Pearson's correlation and agglomerative hierarchical cluster analysis for the identification of
20 microplastics in spectral data sets. Finally, we show their applicability by identifying airborne
21 microplastics >4.7 μm in an outdoor particulate matter sample obtained at an urban sampling site in
22 London, United Kingdom. This semiquantitative method will enable the procurement of exposure
23 concentrations of airborne microplastics guiding future toxicological assessments.

24 **Supplementary information**

25 This document includes the expanded and additional methodological explanations, figures and tables
26 produced in compliment to the original article.

27

28

29

30

31

32   **Table of Contents**

46

47

48

49

50

51

52

53

54

55

56

57

58

59

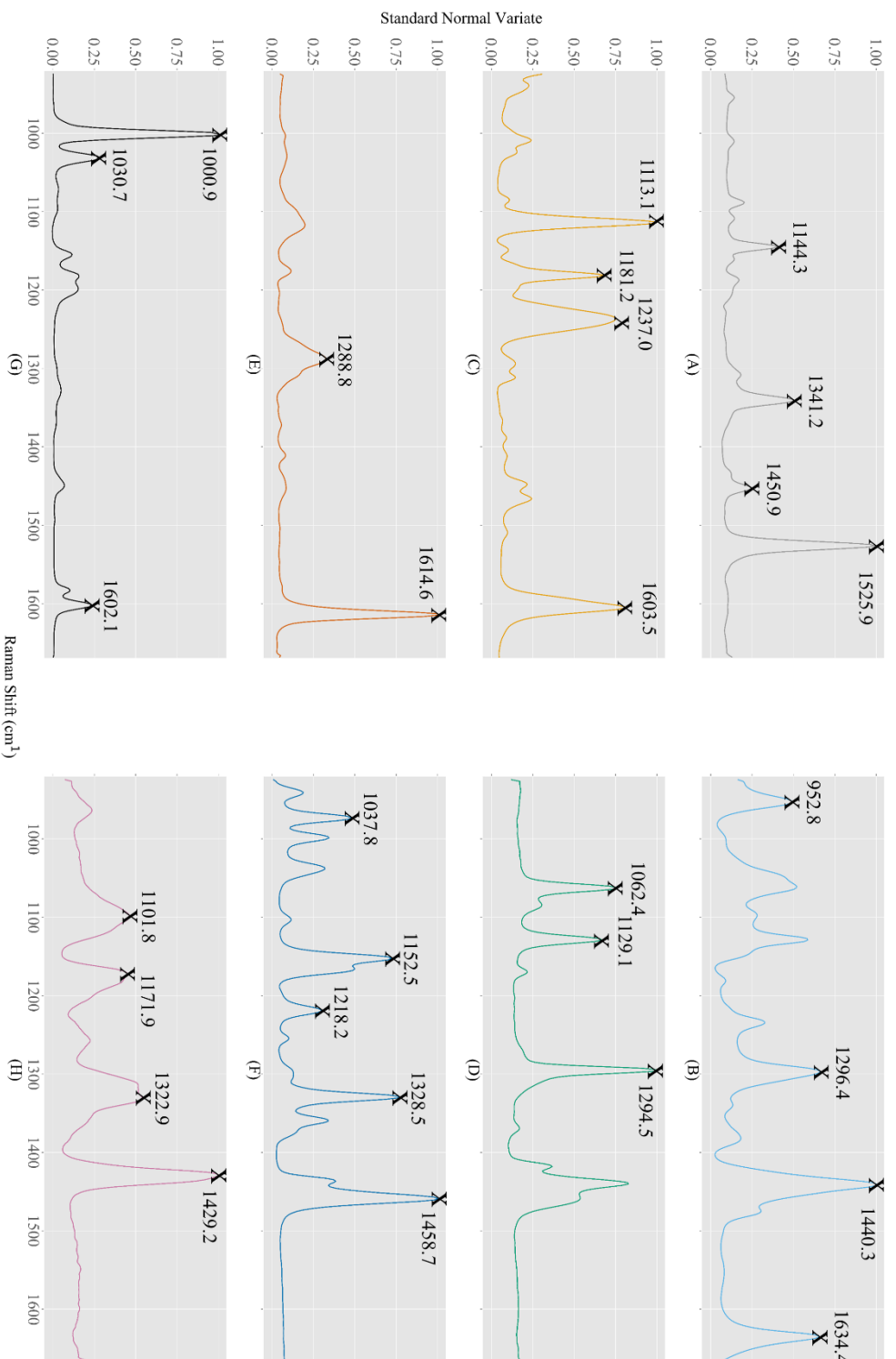60

61

62 **Plastic spectral library**

Figure S1. The mean spectra of Raman spectral images obtained from scanning the surface of common virgin and consumer plastic types and a pigment. (A) copper phthalocyanine; (B) polyamide; (C) polycarbonate; (D) polyethylene; (E) polyethylene terephthalate; (F) polypropylene; (G) polystyrene; and (H) polyvinyl chloride.

87

Spectral data analysis

Pre-processing

Baseline correction parameters were derived from the mean *lambda* and p values assigned to 10 SIs of a blank aluminium slide. Savitzky-Golay filter parameters were chosen as they were found to adequately smooth noise, whilst retaining Raman signal.

Gaussian curve function

The pre-selected characteristic Raman bands, indicative of different plastic compositions is shown in Table S1.

Table S1. Functional group assignment for plastic or pigment spectra contained in the spectral library.

	Minimum energy (cm⁻¹)	Maximum energy (cm⁻¹)	Band (cm⁻¹) energy	Full width at half maximum	Functional group	Reference
Copper phthalocyanine	1099.8	1123.3	1109.6	9.8	Cα–Nα–Cα,Cu–Nα,Cβ–Cγ–H	1
	1133	1158.3	1144.7	9.8	Nα–Cα–Nβ,Cβ–Cγ–H,Cδ–Cδ–H	
	1294.3	1317	1307.6	9.4	Cβ–Cγ–H, Cγ–Cδ–H	
	1328.4	1356.4	1343.3	10.3	Cβ–Cδ,Cα–Cβ–Cδ,Cγ–Cδ,Cβ–Cγ	
	1440.1	1467.7	1451.1	8.7	Cα–Nβ,Nα–Cα–Cβ,C–C–H	
	1518.9	1546.1	1531.6	8.2	Cα–Nβ	
Polyamide	930.7	972.9	952.8	15.1	vC-CO	2
	1113.5	1146.7	1129.1	10.2	-	
	1220.1	1250.8	1233.6	12.8	ωNH2	
	1271.7	1324.7	1296.5	19	tCH2	
	1407	1469.7	1440.9	22.1	σCH2	
	1609.3	1668	1634.4	17.5	Amide I (vC=O)	
Polycarbonate	1093.5	1136.5	1113.1	15.9	vC-O-C	3
	1159.8	1204.3	1181.2	32.9	ωCH	3
	1208.2	1273.2	1235	34.5	vC-O	3
	1571.1	1646.3	1605.3	24.2	vC=C	4
Polyethylene	1044.6	1074.2	1062.4	10	vC-C	5
	1111.6	1142.8	1129.1	10.5	vC-C	
	1279.3	1309.7	1294.5	9.7	tCH2	
Polyethylene terephthalate	1250.8	1330.4	1288.8	31.9	vC-C (ring), vC-O	6
	1593.1	1630.7	1614.6	22.1	vC=C (ring)	
Polypropylene	924.6	952.8	940.7	10.4	tCH2 + vC-C chain	7
	954.8	984.9	972.9	11.9	tCH3 + vC-C chain	
	986.9	1012.8	998.9	9	tCH3 = ωCH2 + δCH	
	1016.8	1058.5	1037.8	15.9	vC-CH3 + vC-C + δCH	
	1191.3	1237.4	1218.2	12.7	tCH2 + δCH + vC-C	
	1311.5	1347.3	1328.5	11.8	-	

98 **Table S1.** (*Continued*)

	Minimum energy (cm⁻¹)	Maximum energy (cm⁻¹)	Band energy (cm⁻¹)	Full width at half maximum	Functional group	Reference
Polypropylene	1347.3	1369.8	1358.5	9.4	CH$_3$ sym ben + σCH$_2$	7
Polystyrene	976.9	1016.8	1000.9	10	ν(C–C) aromatic ring breathing	8
	1018.8	1048.6	1030.7	11.3	δ(CH) aliphatic and aromatic	
	1589.5	1620	1602.1	10.4	ν(C=C) aromatic ring	
Polyvinyl chloride	1054.5	1142.8	1101.8	45	ν(C–C)	9
	1146.7	1225.9	1171.9	32.9	δ(CH$_2$)	9
	1285	1397.7	1322.9	47.1	(CH) out-plane bending	9
	1405.2	1456.9	1429.2	21.5	CH$_2$ deformation	10

99 σ, bending; t, twisting; ν, stretching; ω, wagging; -, unassigned Raman ban

For each analysed Raman band, a raw grey-scale single-point intensity matrix was generated. Impulse noise artefacts in Gaussian-analysed SIs, which are unrelated to the Raman band of interest, were removed using a median filter (11; 12). The filter being a canonical, nonlinear filter, was set to 3 pixels by 3 pixels (12). Preliminary analysis found that larger (4 x 4) kernel windows began to remove spectral signal associated with the 2 μm PS microspheres and smaller (2 x 2) kernels were unsuccessful at removing noise. SIs were imported into ImageJ and ICY for image analysis, outlined in image analysis section (13). To accentuate the signal-to-noise, the Gaussian analysed SI underwent Raman band thresholding. Look-up tables were ascribed to individual Raman band SI, to aid distinction between the generated signals. The image intensity for the Raman bands 1000.9 cm^{-1} and 1030.4 cm^{-1} was set to 192, and to 171 for the band 1602.0 cm^{-1}. Image intensity figures were formulated from the average of 10 SIs of PS particles, which were appropriately corrected to improve distinction between signal and noise. The three Raman band images were merged into a composite image and analysed as outlined in image analysis section. This was conducted for all plastics in the plastic spectral library (Table S2).

Table S2. Raman band image thresholding parameters for each plastic or pigment in the spectral library.

	Band energy (cm^{-1})	Raman band threshold score	Assigned colour palette
Copper phthalocyanine	1109.6	90	Green
	1144.7	150	Blue
	1307.6	50	Grey
	1343.3	250	Cyan
	1451.1	120	Magenta
	1531.6	250	Yellow
Polyamide	952.8	*	-
	1129.1	*	-
	1233.6	*	-
	1296.5	*	-
	1440.9	230.3	Grey
	1634.4	110.2	Cyan
Polycarbonate	1113.1	218	Green
	1181.2	190	Blue
	1235	181	Grey
	1605.3	176	Cyan
Polyethylene	1062.4	199.0	Green
	1129.1	*	-
	1294.5	224	Blue
Polyethylene terephthalate	1288.8	*	-
	1614.6	450	Green
Polypropylene	940.7	395.9	Green
	972.9	487.9	Blue
	998.9	*	-
	1037.8	*	-
	1218.2	504.9	Grey
	1328.5	334.9	Cyan
	1358.5	400	Magenta

114 **Table S2**. *(Continued)*

	Band energy (cm⁻¹)	Raman band threshold score	Assigned colour palette
Polystyrene	1000.9	192	Magenta
	1030.7	192	Green
	1602.1	171	Blue
Polyvinyl chloride	1101.8	*	-
	1171.9	*	-
	1322.9	*	-
	1429.2	80	Magenta

115 * denotes Raman bands with a significant overlap with plastics of a differing composition.

116 **Pearson's correlation coefficient**

117 PCC was conducted in python and utilised the python libraries numpy (14), pandas (15), matplotlib

118 (16), and seaborn (17). For PCC analysis the equation used to determine the monotonic relationship

119 between an unknown spectrum in a spectral image and that of a reference spectrum in the spectral

120 library is shown in equation 1-1.

$$r = \frac{n(\Sigma xy) - (\Sigma x)(\Sigma y)}{\sqrt{[n \sum x^2 - (\Sigma x)^2][n \sum y^2 - (\Sigma y)^2]}}$$

Equation 1-1

121 where r denotes the Pearson's correlation coefficient between x denoting the known plastics reference

122 Raman spectra, and y is the unclassified spectrum in an SI. This equation is iterated over every spectrum

123 in the SI. The colour palette "RdBu_r" was applied to the PCC analysed SI using the Seaborn library

124 (17).

125 **Image analysis**

126 The UDWT which produces a multi-resolution representation of an image. A convolution filter smooths

127 the response of too narrow objects at an operator-defined scale (18). Wavelet coefficients for signal

128 generating PM are high and non-significant values represent the background or large structures

129 (operator defined; 18). To define the scale-dependent threshold a k-hard threshold technique is used.

130 This image is converted to a coefficient correlation image between the values in the correlation image

131 to a predetermined detection level, which enables the identification of signal from the background (18).

132 The mean of all the image channels are processed with the spot detector set to 100% sensitivity for

133 object sizes of ~3 and ~7 pixels and a size filter applied to detect objects from a minimum pixel size of

134 10 to a maximum of 3000. The minimum and maximum pixel size was set to ensure impulse noise and

135 the image background was not included in particle counts.

136 For the proposed chemometric techniques, differing size determination methodologies for the identified

137 microplastics were used. The identified positive signal was sized based on pixel number in both the Y

138 (longest axis), and X (axis perpendicular to longest axis) direction. The number of pixels was converted

139 to micrometre values for AHCA and PCC using Equation 1-2.

$$s = px * sr$$
Equation 1-2

140 where s refers to the size of the positive signal (μm) identified by the transect, px is the pixel number,

141 and sr denotes the spatial resolution of the Raman spectral imaging (RSI) i.e. 1.1 or 2.6.

142 For gaussian analysis, the line transect plot is converted to a profile plot in ImageJ, which displays the

143 pixel intensity distribution along the transect line (13). The raw data of the profile plot is fit using the

144 Gaussian equation shown in equation 1-3 (13).

$$y = a + (b - a) * e - \frac{(x - c)^2}{2d^2}$$
Equation 1-3

145 where b refers to the peak amplitude, c is the position of the centre of the peak, and d denotes the

146 Gaussian root mean squared width (13). Using the Gaussian root mean squared (d) and the Gaussian

147 FWHM distribution of 2.3555σ, the size of a particulate identified using Gaussian analysis can be

148 calculated using equation 1-4 (19).

$$s = d * c$$
Equation 1-4

149 where s refers to the size of the positive signal (μm) identified by the transect, d illustrates the Gaussian

150 root mean squared, and c refers to the FWHM constant of 2.3555 σ (19). Table S3, displays the size

151 measurements obtained from photomicrographs and RSI in both the Y and X direction of the PS

152 microspheres.

153 **Table S3.** A comparison of the nominal (photomicrograph) and detected (RSI) size of 2, 4, and 10 μm
154 PS microspheres.

Analysis Type	Size (μm)	Bright field microscopy determined size in X (μm)	RSI signal size in X direction (pixel number)	Bright field microscopy size in Y (μm)	RSI signal size in Y direction (pixel number)
AHCA	2	2.6 ± 0.3	5.7 ± 1.4	2.15 ± 0.4	10.7 ± 1.3
	4	4.6 ± 0.7	9.1 ± 1.5	5.3 ± 1.0	10.4 ± 2.1
	10	9.3 ± 1.6	15.0 ± 2.7	10.6 ± 2.2	25.0 ± 6.2
Gaussian	2	2.6 ± 0.3	2.0 ± 0.9	2.15 ± 0.4	5.5 ± 3.4
	4	4.6 ± 0.7	3.5 ± 1.1	5.3 ± 1.0	6.7 ± 2.3
	10	9.3 ± 1.6	8.6 ± 1.2	10.6 ± 2.2	16.8 ± 2.6
PCC	2	2.6 ± 0.3	3 ± 0.3	2.15 ± 0.4	8 ± 1.6
	4	4.6 ± 0.7	5 ± 1.4	5.3 ± 1.0	12 ± 1.4
	10	9.3 ± 1.6	13 ± 1.2	10.6 ± 2.2	26.3 ± 2.6

155

156 The size measurements shown in table S3 highlight the similarity of measurements acquired in the X

157 direction via nominal and detected methods, while nominal and detected measurements in the Y

158 direction greatly overestimate the size of the analysed PS microspheres due to the elongation artefact

159   resulting from line-scanning. Therefore, for sphere like particulates sizing in the X direction will
160   produce more accurate sizes.

161   Not only does the direction of measurement influence the observed sizes, but so too does the utilised
162   chemometric technique. The sizes observed following the application of Gaussian and PCC
163   chemometric techniques were closer to the nominal- and photomicrograph-derived PS microsphere
164   sizes than AHCA.

165   **Performance analysis**
166   **Confusion matrix**

167   The Confusion Matrix utilised the performance metrics: precision and recall. Precision (P) is the
168   proportion of true positives (tp) divided by the total number of positive elements i.e. low precision
169   indicates a high number of false positive (fp) classifications (Equation 1-5; 20).

$$P = \frac{tp}{(tp + fp)}$$ Equation 1-5

170   Recall (R) is the proportion of true positives divided by the total number of positive class elements i.e.
171   a high recall infers a high number of true positives, while a low recall infers a high number of false
172   negatives (fn) (Equation 1-6; 20).

$$R = \frac{tp}{(tp + fn)}$$ Equation 1-6

173   Fβ measure has been utilised to compare the prediction accuracy of the proposed chemometric
174   techniques (21). Fβ measure obtains the weighted mean of precision and recall, where +1 refers to a
175   maximal similarity and 0 indicates a dissimilarity between the observation and prediction result for the
176   chemometric technique. The β value determines the weight given to precision or recall results i.e. the
177   greater β value the more importance is attributed to precision (13;22). As the precision of the proposed
178   chemometric techniques was deemed of increased importance β was set to 0.95 (Equation 1-7).

$$F_\beta = \frac{1}{\left(\left(0.95 * \left(\frac{1}{P}\right)\right) + \left((1 - 0.95) * \left(\frac{1}{R}\right)\right)\right)}$$ Equation 1-7

179

180   **Preparation of PS microsphere working samples**

181   The PS microspheres were procured from the Spherotech Inc or Sigma at 5 or 10% weight per volume
182   concentrations, respectively. The approximate particle number for each size range was calculated from
183   the weight per volume concentrations using equation 1-8.

$$\text{p/mL} = \frac{S * (6 * 10^{10})}{\pi * p_p * D^3}$$ Equation 1-8

184 where p/mL denotes the microsphere number/mL for suspensions in water, S weight % of solids in

185 suspension for 10% S equates to 10, p_p is the microsphere density (g/cm^3) i.e. 1.055 for PS, and φ is

186 the mean diameter (μm). This calculation determined the particle per mL concentration to be 1.81 *

187 10^{11}, 2.26 * 10^{10}, 1.26 * 10^9, and 1.81 * 10^8 per mL for 1, 2, 4, and 10 μm PS microspheres, respectively.

188 The 2, 4, and 10 μm PS microspheres were diluted 1 in 100 000, 1 in 10 000, and 1 in 1 000 to generate

189 2.26 * 10^5, 1.26 * 10^5, 1.81 * 10^5 per mL concentrations. From these diluted samples 44.2, 79.4, and

190 55.2 μL aliquots were acquired and resuspended in EtOH to generate 1 x 10^4 microspheres/mL

191 concentrations. A further 1 in 10 dilution was conducted on such working samples (1 x 10^4

192 microspheres/mL) and a 10 μL aliquot was obtained, dispensed into a haemocytometer chamber and

193 counted under a microscope. To control for pipetting fluctuations haemocytometer counts were

194 conducted thrice for each microsphere size and the precision of the dilution series was displayed using

195 the standard deviation from the mean particle counts. The results for which are presented in the Table

196 1 as expected concentrations illustrating the mean and standard deviation of the three microsphere

197 counts. The expected concentrations are the back-calculated values from the haemocytometer counts

198 which represent the spiked particle number concentration.

199 **PS spiked ambient particulate matter sample preparation**

200 Due to the dried drop cast's area being relatively large and concerns over file size, the SI was acquired

201 in 6 separate units at ~2.6 μm spatial resolution. The Raman scan duration and dimensions of each SI

202 unit are shown in Table S4. Each individual SI unit once analysed was tiled together to generate a

203 sample wide SI. The Raman scan duration and dimensions of each SI captured at ~2.6 μm spatial

204 resolution is displayed in Table S4.

205 **Table S4.** The image parameters i.e. size (X and Y), spectra number, scan duration, and analysis time

206 for SIs obtained ~2.6 μm spatial resolution of the spiked ambient particulate matter sample.

RSI section number	X dimension (μm)	Y dimension (μm)	Number of spectra	Scan duration (hours)	Analysis time (min)		
					AHCA	**Gaussian**	**PCC**
1	3848	540.8	307 840	8	5	11	18
2	3835	1003.6	569 350	10	6	46	31
3	5005	1003.6	743 034	13	39	49	27
4	5005	1003.6	743 050	13	31	82	37
5	5005	1003.6	743 050	13	16	34	13
6	4204.2	803.4	499 653	9	29	47	15

207

208 The Raman scan duration and dimensions of each SI captured at ~1.1 μm spatial resolution is displayed

209 in Table S5.

Table S5. The image parameters i.e. size (X and Y), spectra number, scan duration, and analysis time for SIs obtained at ~1.1 μm spatial resolution of the spiked ambient particulate matter sample.

RSI section number	X dimension (μm)	Y dimension (μm)	Number of spectra	Scan duration (hours)	Analysis time (min)		
					AHCA	Gaussian	PCC
1	641.3	821.7	435 501	11	1064	44	11
2	829.4	662.2	453 908	11	450	39	15
3	828.3	790.9	541 407	13	713	91	14
4	668.8	788.7	435 936	10	684	53	11
5	662.2	754.6	412 972	10	849	20	12
6	699.6	883.3	510 702	12	604	64	14

For AHCA there was a marked increase in the analysis time for RSI obtained at ~1.1 μm in comparison to ~2.6 μm spatial resolution (Table S4, S5), this is hypothesized to be due to an increased complexity of contained spectral information.

Sample wide concentration determination for ~1.1 μm spectral images

The PS microspheres and environmental microplastics identified in the SIs obtained at ~1.1 μm spatial resolution were back calculated to produce sample-wide particle concentrations using equation 1-9.

$$N = sf * \overline{N} \qquad \text{Equation 1-9}$$

where sf is the scaling factor determined by $sf = \frac{100}{sA}$ where sA denotes the scanned area defined by

$sA = \frac{\left(\frac{s}{st}\right)*100}{N}$ where s refers to the total scanned area in ~1.1 μm SIs, st is the total sample area, N is the number of SIs acquired, and $\overline{N}$ is the mean particle number across the analysed SIs. The standard deviation of N is determined using Equation 1-10.

$$\sigma = sf * \overline{\sigma} \qquad \text{Equation 1-10}$$

where sf is the scaling factor, and $\overline{\sigma}$ is the standard deviation of the particle counts across every SIs.

Airborne microplastic concentration

The number of spectroscopically identified airborne microplastics was back calculated to estimate a sample-wide concentration. The extracted subsample used for preparing the ambient spiked PM sample (312 μg), represented 37.1% of the original 24-hr PM_{10} sample mass (841.68 μg). To extrapolate microplastic counts to the whole sample equation 1-9 was used.

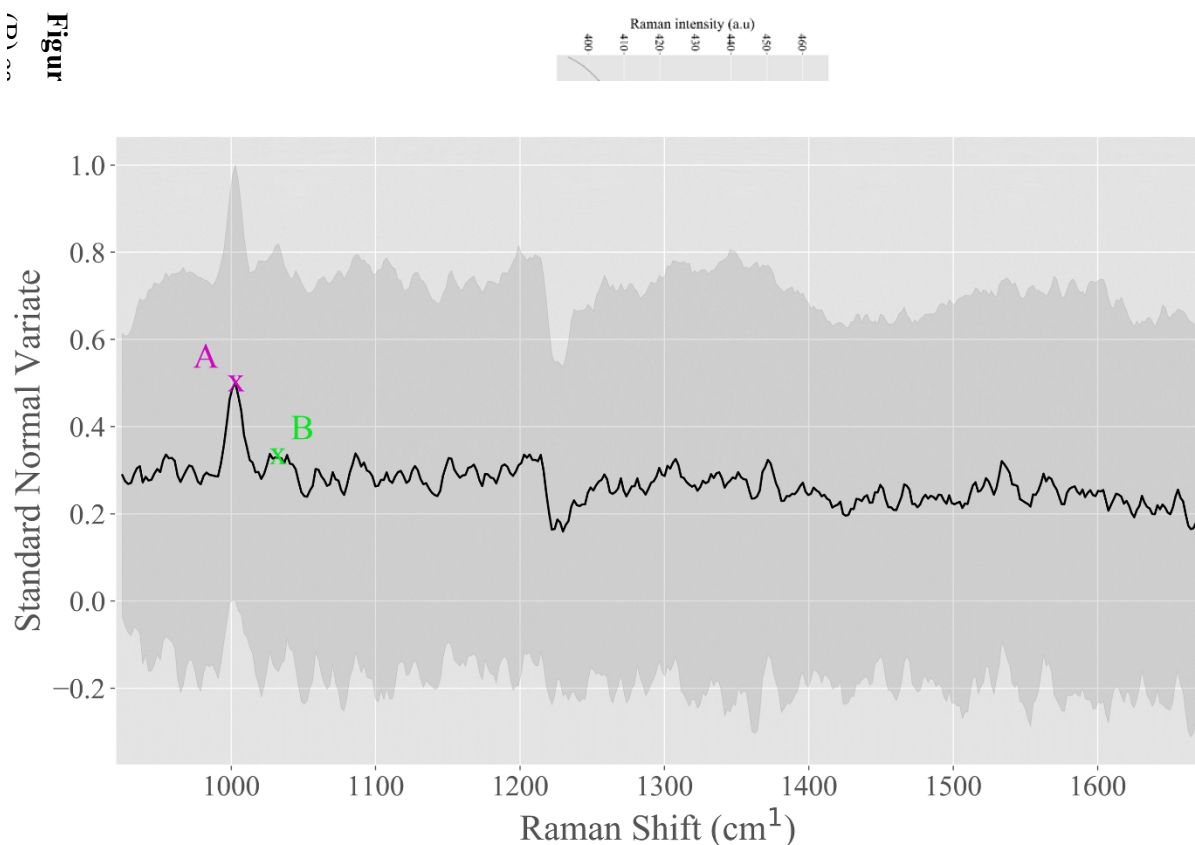$$MP = sMP * dc \qquad \text{Equation 1-11}$$

229 where MP denotes the sample wide concentration of airborne microplastics, sMP refers to the

230 subsample microplastic particle number, and dc is the dilution constant of 2.69.

231 The chemometric techniques identification rates for microplastics in simple spectral images (SI)

232 obtained at ~1.1 and ~ 2.6 µm spatial resolution were compared using a confusion matrix (Table S6).

233 **Table S6.** Confusion matrix analysis i.e. precision and recall, of the proposed chemometric techniques

234 was conducted based on classification rates of spectral images (SI) of the different sized microspheres,

235 EtOH evaporates, and the aluminium slide (blank). SIs of 4 and 10 µm PS microspheres were obtained

236 at ~2.6 µm and SIs of 1, and 2 µm PS microspheres were obtained at ~1.1 µm. The SI were analysed

237 for the presence of polystyrene's Raman spectrum or it's associated Raman bands.

Chemometric analysis type	Sample	Precision	Recall
AHCA	Aluminium slide	0	0
	EtOH evaporates	0	0
	1µm:	0	0
	2µm:	1.0	0.9
	4µm:	1.0	0.9
	10µm:	1.0	1.0
Gaussian	Aluminium slide	0	0
	EtOH evaporates	0	0
	1µm:	0	0
	2µm:	0	0
	4µm:	0	0
	10µm:	1.0	1.0
PCC	Aluminium slide	0	0
	EtOH evaporates	0	0
	1µm:	0	0
	2µm:	1.0	0.9
	4µm:	1.0	0.9
	10µm:	1.0	1.0

238

239

240

241

242

243

244

245

246

Raman band A
Band Energy: 1000.9
Minimum Energy: 976.9
Maximum Energy: 1016.8
FWHM: 10.0

Raman band B
Band Energy: 1030.7
Minimum Energy: 1018.8
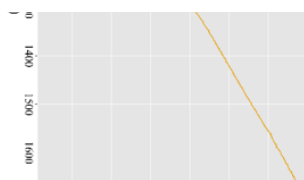Maximum Energy: 1048.6
FWHM: 11.3

Figure S3. The mean (black) and standard deviation (grey) of 1 μm polystyrene (PS) microspheres Raman spectra (n=30) acquired using Raman Spectral Imaging, annotated for the presence of the PS associated Raman bands 1000.9 cm^{-1} (magenta), and 1030.7 cm^{-1} (blue). The Raman band at 1602.1 cm^{-1} is completely suppressed and not present in the Raman spectrum.
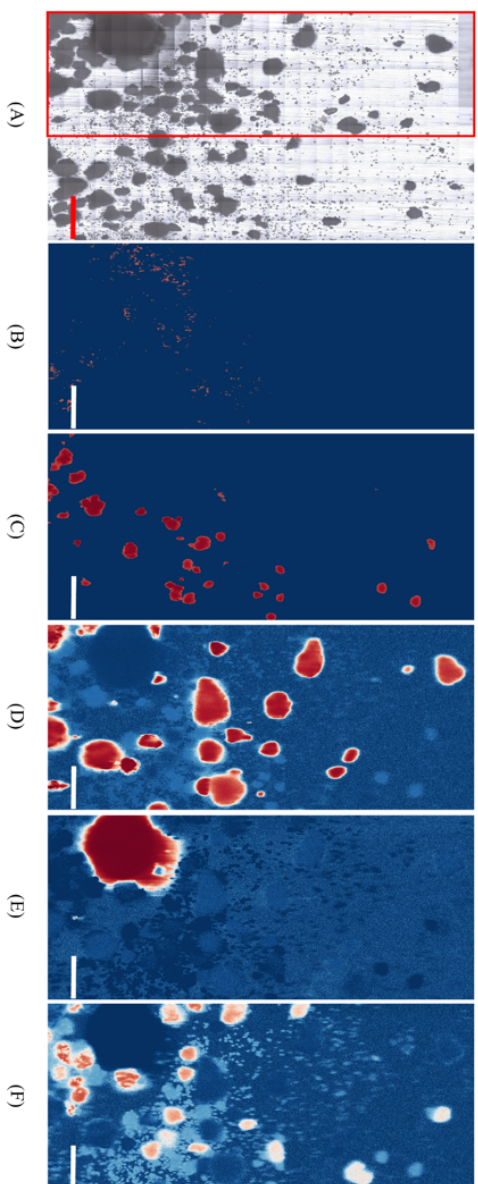
Figure S4. Raman spectral images of virgin microplastics dried on to an aluminium slide. (A) A micrograph of a virgin microplastic mixture dried on to an aluminium slide. The approximate spectral image (SI) area is outlined in red. (B – F) PCC analysis of the SI identified polyamide (B), polyethylene (C), polyethyleneterephthalate (D), polystyrene (E), and polyvinyl chloride (F). The
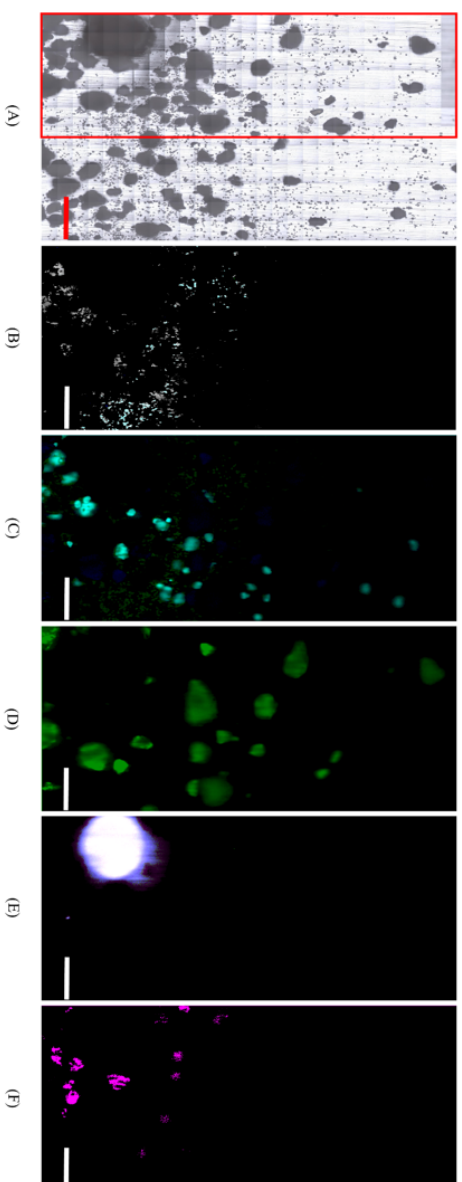
Figure S5. A Raman spectral image of virgin microplastics on an aluminium slide, analysed using Gaussian analysis (A; approximate spectral image area is shown in red). The spectral image was analysed for plastic related Raman bands, and for each Raman band a pixel intensity threshold was applied, described in Table S2. Raman band spectral images were assigned a colour lookup table, interlaced into plastic composite images, and investigated for microplastic content. The identified microplastics were composed of polyamide (B), polyethylene terephthalate (D), polystyrene (E), and polyvinyl chloride (F). Scale bar: 500 μm.
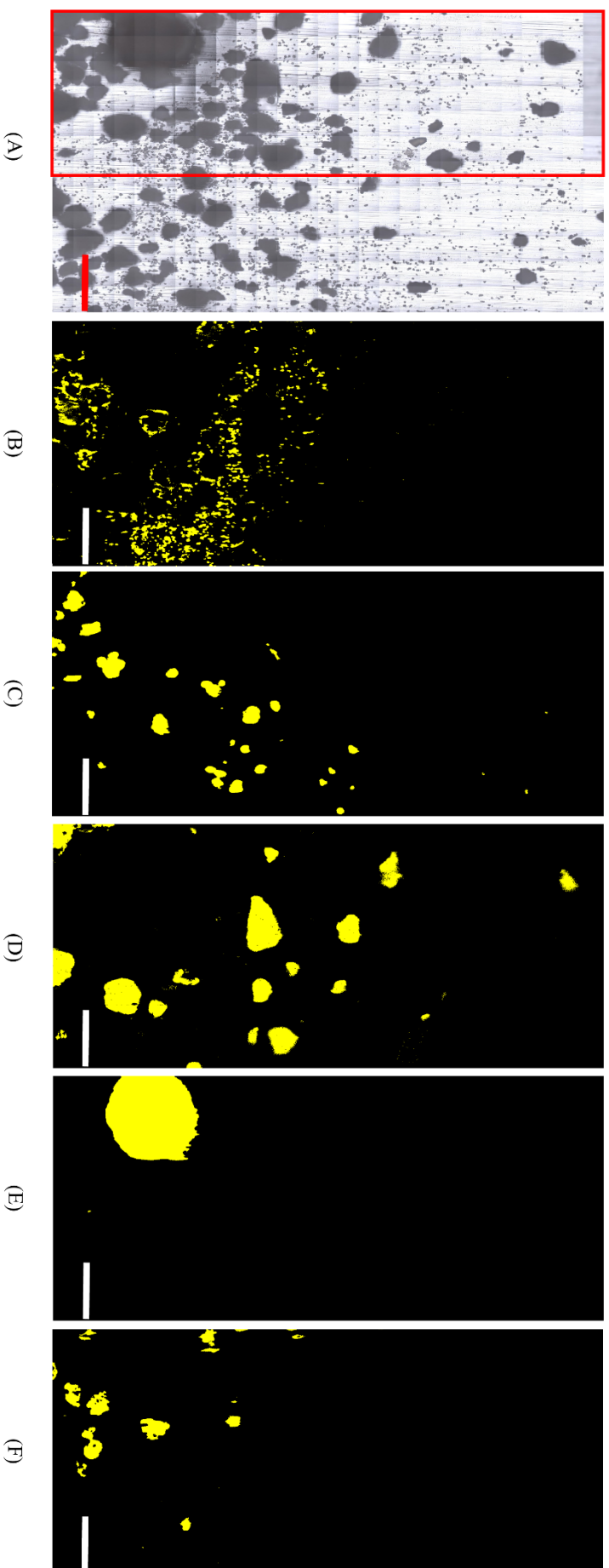
Figure S6. Agglomerative hierarchical cluster analysis of a Raman spectral image of virgin microplastics deposited on an aluminium slide (A; approximate Spectral image area is shown in red). The identified plastic related clustered spectral images were ascribed a yellow colour lookup table, where yellow shows the presence and black the absence of a plastics Raman spectrum. Identified microplastics were composed of polyamide (B), polyethylene (C), polyethylene terephthalate (D), polystyrene (E), and polyvinyl chloride (F). Scale bar: 500 µm.
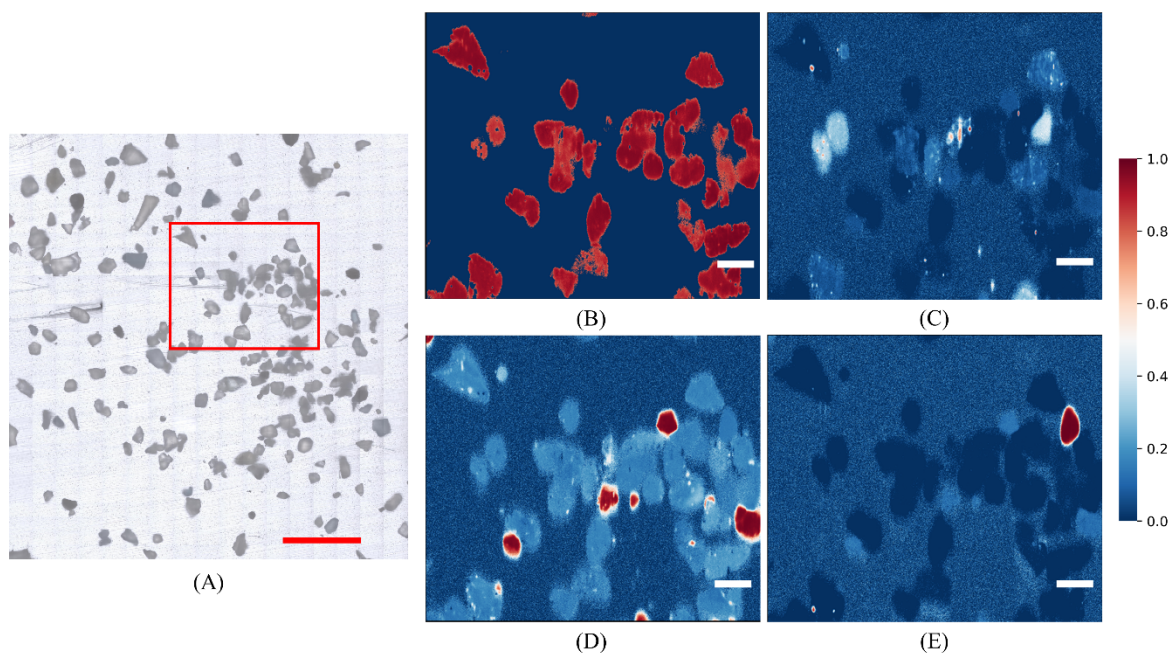
334

Figure S7. Raman spectral images of environmental microplastics dried on to an aluminium slide. (A) A micrograph of environmental microplastics dried on to an aluminium slide (scale bar: 1000 μm). The approximate SI area is outlined in red. PCC analysis identified polyethylene (B), copper phthalocyanine (C), polypropylene (D), and polystyrene (E). The pixels shown in red, refer to positive correlations, while blue denotes the corrected negative or independent correlations (0; Scale bar: 250 μm).
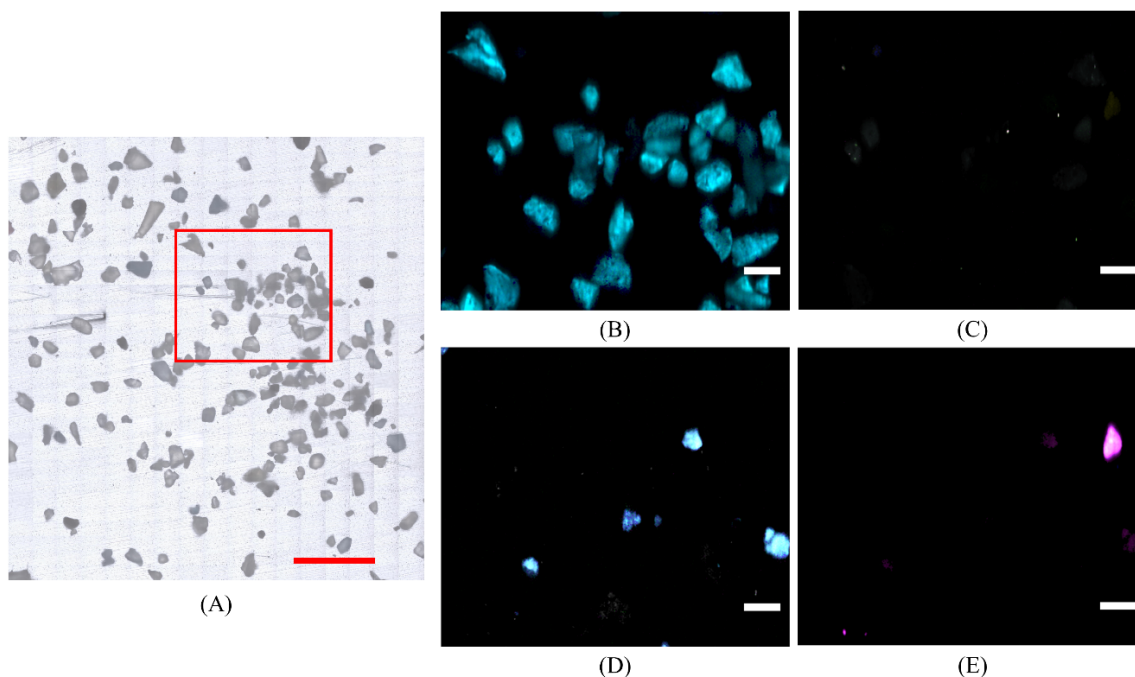
340

341

342

343

344

345

346

347

348

349

350

351

(A)

(B)

(C)

(D)

(E)

Figure S8. Raman spectral images of environmental microplastics dried on to an aluminium slide. (A) A micrograph of environmental microplastics dried on to an aluminium slide (scale bar: 1000 μm). The approximate SI area is outlined in red. Gaussian analysis for Raman bands in a plastic or pigments spectra are interlaced based on composition, a pixel intensity threshold was applied to accentuate areas of positive signal (Table S2). Identified microplastics were composed of polyethylene (B), copper phthalocyanine (C), polypropylene (D), and polystyrene (E). The plastic related Raman bands used are present in Table S2. Scale bar: 250 μm.
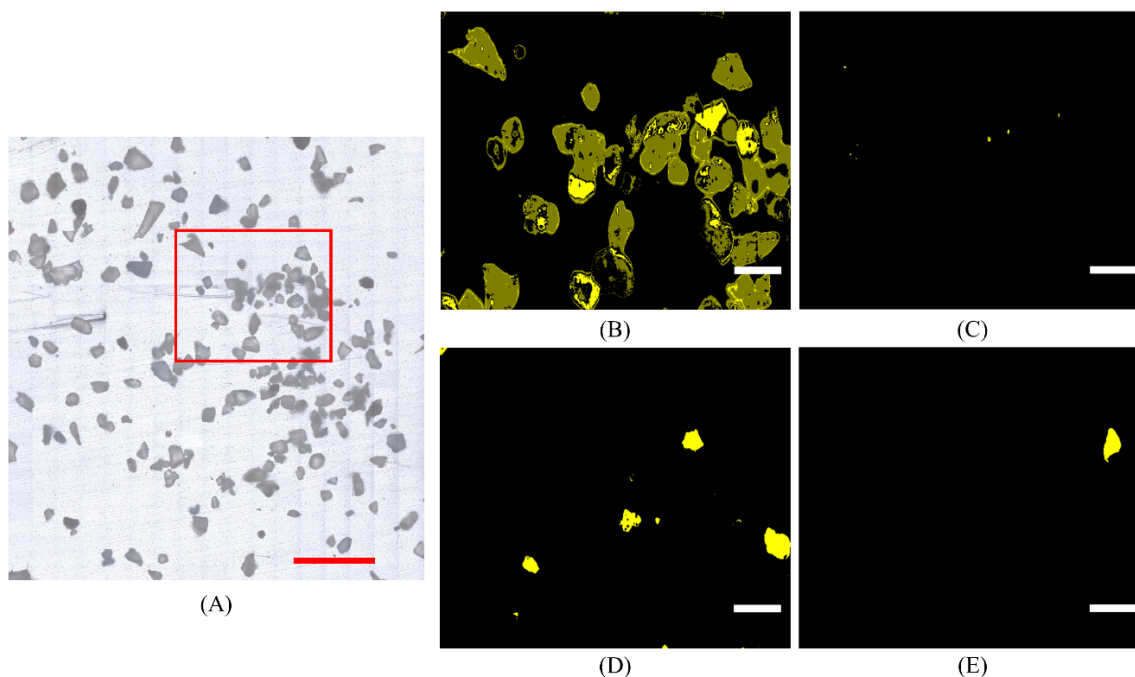
(A)

(B)

(C)

(D)

(E)

Figure S9. Raman spectral images of environmental microplastics dried on to an aluminium slide. (A) A micrograph of environmental microplastics dried on to an aluminium slide (scale bar: 1000 μm). The approximate SI area is outlined in red (A; scale bar: 1000 μm). Agglomerative Hierarchical Cluster Analysis of a Raman spectral image containing environmental microplastics deposited on an aluminium slide. The spectral clusters identified as having a plastic associated Raman spectrum were imaged and ascribed a colour lookup table, where yellow shows the presence and black the absence of a plastics Raman spectrum. The identified microplastics were composed of polyethylene (B), copper phthalocyanine (C), polypropylene (D), and polystyrene (E). Scale bar: 250 μm.
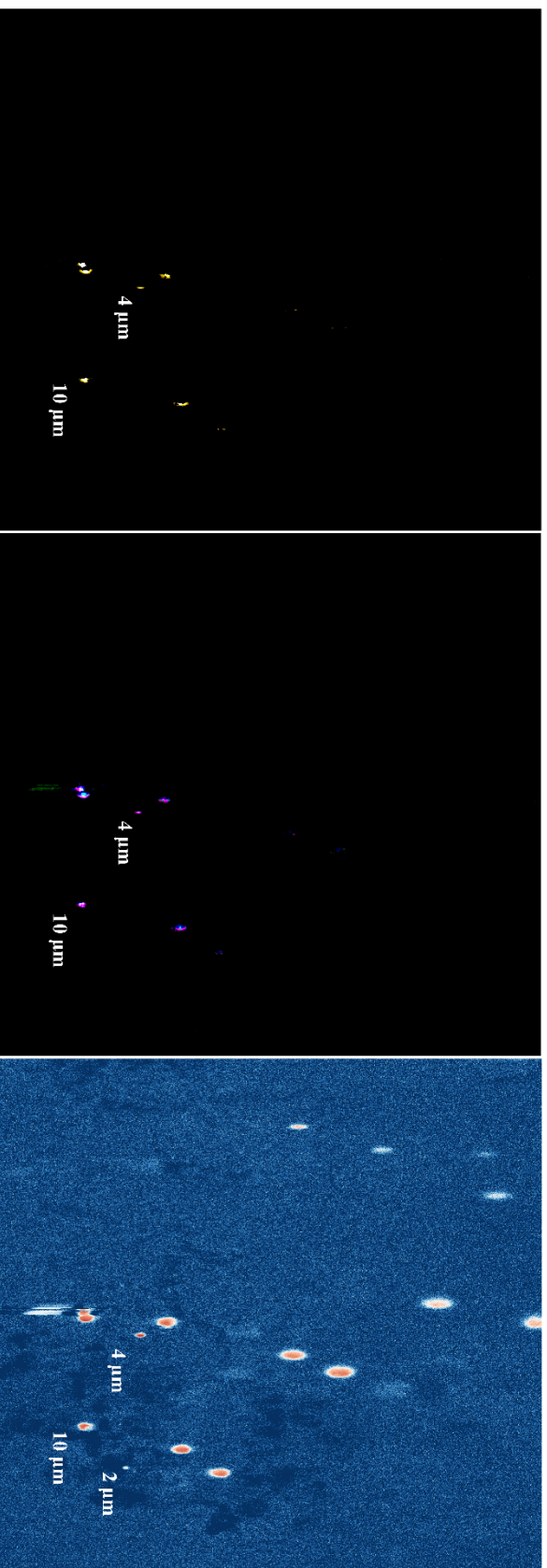
Figure S10. The polystyrene (PS) spiked PM sample dried on an aluminium slide was analysed using Raman spectral imaging (RSI) at 2.6 µm and 1.1 µm spatial resolution. The generated spectral images (SI) were investigated for the presence of PS's Raman spectral fingerprint or characteristic bands using the proposed chemometric techniques. A subsection of the sample analysed at 1.1 µm spatial resolution is shown in A, B, and C. Agglomerative Hierarchal Cluster Analysis (A) identified the spectral clusters corresponding to PS's spectrum, yellow pixels denote the presence and black pixels refer to the absence of PS's spectrum. Gaussian analysis identified the 3 Raman bands in PS Raman spectrum (B). The SIs analysed for individual Raman bands were interlaced and colour coded (magenta corresponding to the Raman band at 1000.9 cm^{-1}, green to 1030.7 cm^{-1} and blue 1602.1 cm^{-1}) generating a Gaussian SI (B). To enhance positive Raman band signal the Gaussian analysed SIs were set to maximum pixel intensities of 192, 192, and 175. Pearson's Correlation Coefficient analysis illustrates a positive correlation (1.0) in red, while blue pixels refer to negative or independent correlations (0.0; C). The areas of positive Raman signal referring to 2, 4, and 10 µm PS microspheres were annotated in the produced SIs.
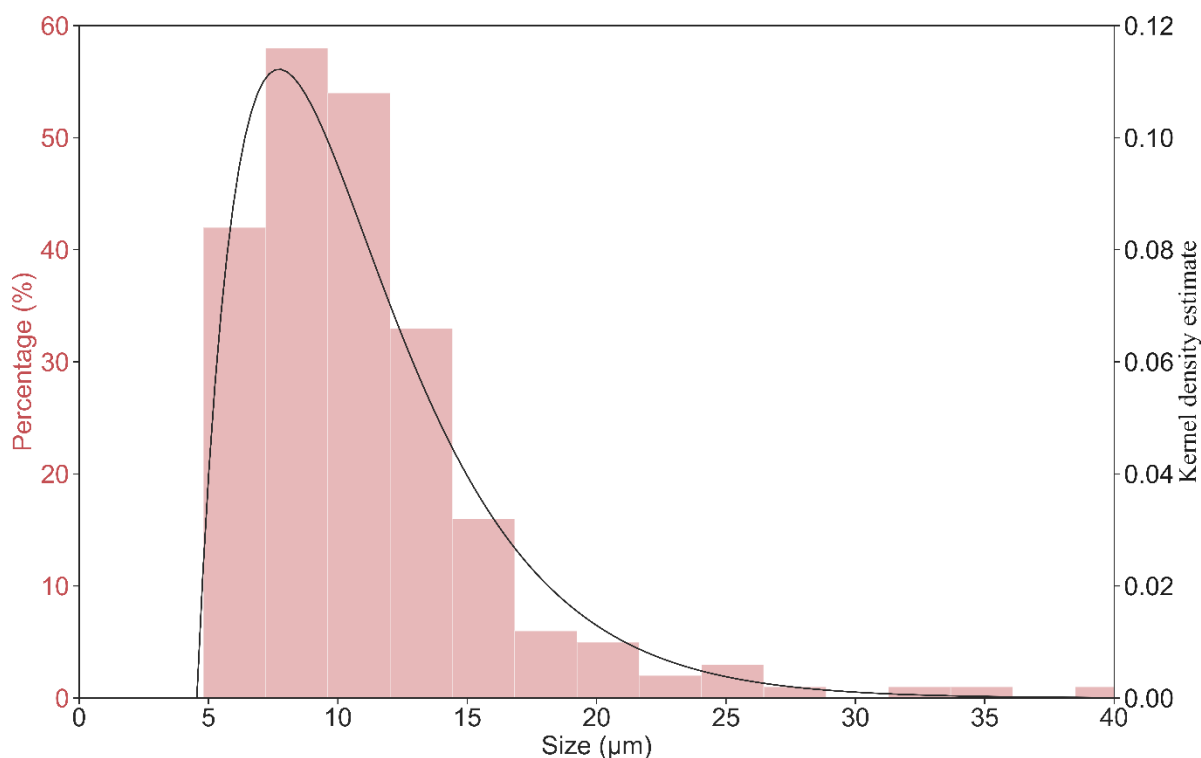
387
388
389
390
391
392
393
394
395
396
397
398
399
400
401
402
403
404
405
406
407
408

Figure S11. Size distribution of identified environmental airborne microplastics. The kernel density estimate, illustrated as the line plot, demonstrates the probability density per particle size bin.

Table S7. Environmental microplastics identified in the Spiked PS ambient sample.

Plastic type	Count	Sample-wide microplastic concentration (n/m³)	Mean Size (μm)	Size range (μm)
Polyethylene	220	2467.9	11.0 ± 5.0	4.7 – 40.9
Polypropylene	2	22.4	13.7 ± 5.2	10.0 – 17.4
Polyethylene terephthalate	1	11.2	22	-

416

References

1. Basova, T.; Kiselev, V.; Schuster, B.; Peisert, H.; Chassé, T. *J. Raman Spectrosc.* **2009**, 40 (12), 2080 – 2087.

2. Hendra, P.; Maddams, W.; Royaud, L.; Willis, H.; Zichy, V. *Spectrochimica Acta Part A: Molecular Spectroscopy* **1990**, 46 (5), 747 – 756.

3. Lee, S.; Stolarski, V.; Letton, A.; Laane, J. *J. Mol. Struct.* **2000**, 521 (1 – 3), 19 – 24.

4. Bia, L.; Gigant, K.; Posset, U.; Schottner, G.; Kiefer, W.; Popp, J. *Appl. Spectrosc.* **2002**, 56 (4), 536 – 540.

5. Sato, H.; Shimoyama, M.; Kamiya, T.; Amari, T.; Šašic, S.; Ninomiya, T.; Siesler, H.; Ozaki, Y. *J. Appl. Polym. Sci.* **2002**, 86 (2), 443- 448.

427 6. Bistričić, L.; Borjanović, V.; Leskovac, M.; Mikac, L.; McGuire, G.; Shenderova, O.; Nunn, N.
428   *J. Polym. Res.* **2015**, 22 (3), 39.

429 7. Arruebarrena de Báez, M.; Hendra, P.; Judkins, M. *Spectrochim. Acta, Part A* **1995**, 51 (12),
430   2117 – 2124.

431 8. Winkler, M.; Musso, M.; Kirchner, E. *J. Raman Spectrosc.* **2003**, 34 (2), 157 – 162.

432 9. Klisińska-Kopacz, A.; Łydżba-Kopczyńska, B.; Czarnecka, M.; Koźlecki, T.; del Hoyo
433   Mélendez, J.; Mendys, A.; Kłosowska-Klechowska, A.; Obarzanowski, M.; Frączek, P. *J.*
434   *Raman Spectrosc.* **2019**, 50 (2), 213 - 221.

435 10. Rusen, E.; Marculescu, B.; Butac, L.; Preda, N.; Mihut, L. *Fullerenes, Nanotubes, Carbon*
436   *Nanostruct.* **2008**, 16 (3), 178 - 185.

437 11. Tukey, J. *Exploratory Data Analysis*, 1st ed.; Addison-Wesley: Menlo Park, CA, 1977.

438 12. Ahmed, E.; Elatif, R.; Alser, Z. *International Journal of Signal Processing, Image Processing*
439   *and Pattern Recognition* **2015**, 8 (10), 343 - 352.

440 13. Schindelin, J.; Arganda-Carreras, I.; Frise, E.; Kaynig, V.; Longair, M.; Pietzsch, T.; Preibisch,
441   S.; Rueden, C.; Saalfeld, S.; Schmid, B.; Tinevez, J.; White, D, J.; Hartenstein, V.; Eliceiri, K.;
442   Tomancak, P.; Cardona, A. *Nature* Methods **2012** 9, 676 - 682.

443 14. Oliphant, T.E. *A Guide to NumPy*; Trelgol Publishing: USA, 2006.

444 15. McKinney, W. Data structures for statistical computing in python. *In Proceedings of the 9th*
445   *Python in Science Conference*, 201, 56 - 61.

446 16. Hunter, J.C. *Comput. Sci. Eng.* **2007**, 9 (3), 90 - 95.

447 17. Waskorn, M. *Seaborn: Statistical Data Visualization – Seaborn 0.10.0 Documentation, 2020.*
448   *https://seaborn.pydata .org/* (accessed 2020-4-6).

449 18. Olivo-Marin, J. *Pattern Recognition* **2002**, 35 (9), 1989 - 1996.

450 19. Wright, S.; Levermore, J.; Kelly, F. *Environ. Sci. Technol.* **2019**, 53 (15), 8947 - 8956.

451 20. Lenz, R.; Enders, K.; Stedmon, C.; Mackenzie, D.; Nielsen, T. *Mar. Pollut. Bull.* **2015**, 100 (1),
452   82 - 91.

453 21. Powers, D. *Journal of Machine Learning Technologies* **2011**, 2 (1), 37 - 63.

454 22. van Rijsbergen, C. *Information retrieval. 2nd ed.;* Butterworths: London, 1979.

455